Chinese Chemical Letters 35 (2024) 108809

Contents lists available at ScienceDirect

Chinese Chemical Letters

journal homepage: www.elsevier.com/locate/cclet

Two new high-temperature molecular ferroelectrics [1,5-3.2.2-Hdabcn]X ($X = ClO_4^-$, ReO_4^-)

Keke Han[a], Wenjun Rao[a], Xiuli You[b], Haina Zhang[a], Xing Ye[a], Zhenhong Wei[a,*], Hu Cai[a,*]

[a] School of Chemistry and Chemical Engineering, Nanchang University, Nanchang 330031, China
[b] Jiangxi Key laboratory of Organic Chemistry, Jiangxi Science and Technology Normal University, Nanchang 330013, China

ARTICLE INFO

Article history:
Received 20 April 2023
Revised 13 June 2023
Accepted 12 July 2023
Available online 14 July 2023

Keywords:
Ferroelectric domains
Quasi-spherical amine
Phase transition
Polarization

ABSTRACT

Molecular ferroelectrics have attracted much attention because of their excellent piezoelectricity, mechanical workability, and second harmonic effect. Here, we successfully prepared two molecular ferroelectrics [1,5–3.2.2-Hdabcn]X ($X = ClO_4^-$, **1**; ReO_4^-, **2**) by reactions of a *quasi*-spherical amine 1,5-diazabicycle[3.2.2]nonane (1.5–3.2.2-dabcn) with HX aqueous solution. Compounds **1** and **2** undergo high-temperature phase transitions at 381 K (**1**) and 396 K (**2**). Before and after the phase transition, they crystallize in the polar point group *mm*2, and the centrosymmetric point groups *mmm* and 4/*mmm*, respectively. According to Aizu rules, these two compounds experience *mmmFmm*2 and 4/*mmmFmm*2 type ferroelectric phase transitions, respectively. The ferroelectricity of both compounds is well expressed in their polycrystalline film at room temperature with low coercive voltages of 13 V for **1** and 25 V for **2**. Using piezoelectric force microscopy (PFM), the 180° anti-parallel ferroelectric domains and the reversible polarization switching can be clearly observed in **1** and **2**. This high-temperature molecular ferroelectric material has great application potential in flexible materials, biomechanics, intelligent wearables and other fields.

Ferroelectrics are a class of polar materials with spontaneous polarization and the polarization direction can be reversed under the stimulation of an external electric field [1]. The polarization of ferroelectrics can also change with the change of applied stress, electric field, or temperature, so it can show the physical effects of force, sound, light, electricity, heat, and other interactive responses, thus becoming one of the ideal materials for manufacturing multifunctional devices and sensitive components in the field of high technology [2–7].

Since the discovery of the first ferroelectric Rochelle salt in 1920 [8], ferroelectric development has opened a new era, and more than a thousand ferroelectrics have been introduced so far [9–13]. At present, inorganic ceramic ferroelectrics (BTO, PZT, *etc.*) are still the most widely studied and used [14–21]. However, these materials require high-temperature sintering, which not only has high production cost and high energy consumption but also contains heavy metals posing a serious threat to environmental safety. Therefore, organic molecular ferroelectrics with excellent ferroelectric properties, simple production process, low cost, and environmental friendliness have become important supplements for the traditional inorganic ferroelectric materials [22–24].

Ferroelectrics are often used in practical production and work in the form of ferroelectric thin films and ferroelectric crystals [25–32]. Ferroelectric thin films have great advantages in the expression of piezoelectric properties, ferroelectric domains, electric polarization switching, and so on [33,34].

In the long-term molecular ferroelectric research [35–37], chemists and physicists found that organic ligands as stimulus responsive structural units play an important role in inducing ferroelectric properties [38,39]. Among them, the organic ligand with the spherical structure exhibits plastic characteristics, it is easy to form films and can be processed into various shapes, exhibiting outstanding performance on ferroelectric properties [40]. The typical compounds such as $[(CH_3)_4N]FeCl_4$ [41], $[(CH_3)_4P]CdCl_3$ [42], [1,4–2.2.2-dabco]ReO_4 [37], [1,4–2.2.2-dabco]ClO_4 [43], have been reported.

Combined with our previous work [3.2.1-dabco]BF_4 [44], we designed and synthesized a caged molecule 1,5-diazabicyclo[3.2.2]nonane (1.5–3.2.2-dabcn) with a larger cage structure showing higher molecular rotational energy barrier when compared to 1,5-diazodicyclic[3.2.1]octane (3.2.1-dabco), which is more favorable for inducing high-temperature phase transitions.

* Corresponding authors.
E-mail addresses: weizh@ncu.edu.cn (Z. Wei), caihu@ncu.edu.cn (H. Cai).

https://doi.org/10.1016/j.cclet.2023.108809
1001-8417/

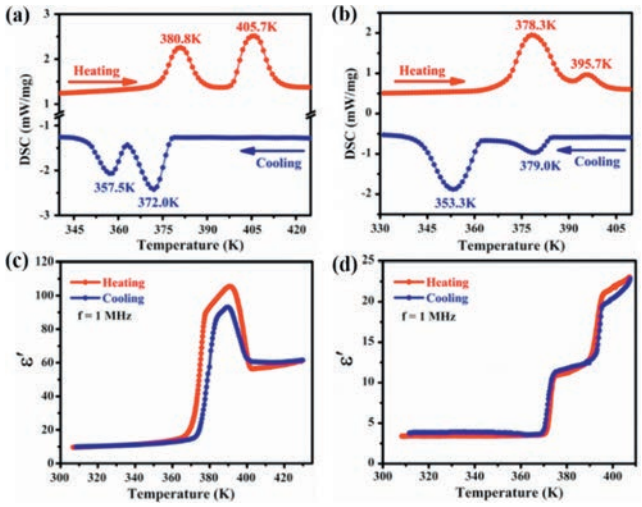

Fig. 1. (a, b) DSC and (c, d) the dielectric constants ε' of compounds **1** and **2** in a heating and cooling cycle.

Reaction of equimolar amounts of 1.5–3.2.2-dabcn with $HClO_4$ or $HReO_4$ in a mixed solution of methanol and water produced two organic-inorganic hybrid crystals [1,5–3.2.2-Hdabcn]ClO_4 (**1**) and [1,5–3.2.2-Hdabcn]ReO_4 (**2**). The single crystal structure analysis showed that both compounds **1** and **2** crystallized in the ferroelectric space groups $Pmn2_1$ and $Pca2_1$, respectively. The obvious ferroelectric domains and polarization direction reversal of compounds **1** and **2** were observed by piezoresponse force microscopy (PFM) at room temperature.

Differential scanning calorimetry (DSC) and dielectric measurement are effective methods to characterize the structural phase transition. As shown in Fig. 1a and Fig. S1 (Supporting information), compound **1** exhibits three reversible phase transitions with the first at the low-temperature region $T_1 = 227/214$ K, and the other two at the above-room temperatures $T_2 = 381/357$ K, $T_3 = 406/372$ K. While compound **2** shows two reversible and high-temperature phase transitions at $T_1 = 378/353$ K and $T_2 = 396/379$ K (Fig. 1b). The large thermal hysteresis ($\Delta T_2 = 33$ K, $\Delta T_3 = 23$ K of **1**; $\Delta T_1 = 25$ K, $\Delta T_2 = 16$ K of **2**) reveals the type of first-order phase transition. The N values in the phase transitions are about 16.71 (T_2) and 18.58 J mol^{-1} K^{-1} (T_3) for **1**, and 42.45 (T_1) and 3.47 J mol^{-1} K^{-1} (T_2) for **2**, indicating that the four pairs of phase transitions are ascribed to the order-disorder type phase transitions.

The phase transition of **1** and **2** was further verified by the temperature-dependent of the real part (ε') of the complex permittivity ε ($\varepsilon = \varepsilon' - i\varepsilon''$, where ε'' is the imaginary part of the permittivity). The ε' of compounds **1** and **2** show two distinct dielectric anomalies near their respective high-temperature phase transition points (Figs. 1c and d), which are consistent with their DSC results. As the temperature increases, the ε' values of **1** increase from 10 to 90 to 106 and then decrease to 56, the high dielectric state is about 10.6 times that of the low dielectric state. The ε' value of **2** increases from 3.4 to 11 and then continues to rise to 21, the maximum value is 6.2 times that of the minimum value.

The T-ε' curve of **1** shows a sharp peak shape, indicating that it may be an intrinsic ferroelectric, while the stepped dielectric anomaly curve of **2** suggests that it is an extrinsic ferroelectric. In addition, compounds **1** and **2** exhibit significant dielectric losses (the imaginary part) at their respective phase transition points at 1 MHz (Figs. S2a and b in Supporting information).

Because both compounds **1** and **2** were found to undergo multiple reversible phase transitions, the variable-temperature X-ray single-crystal diffractions at the different phases were recorded to gain insight into the phase transition mechanism. As shown in Table S1 (Supporting information), the crystal structures of **1** in phase I (173 K, below T_1) and phase II (293 K, between T_1 and T_2) are crystallized in the orthorhombic system, with the polar space groups $Pna2_1$ and $Pmn2_1$ (point group $mm2$), meeting the symmetry requirement for ferroelectrics,

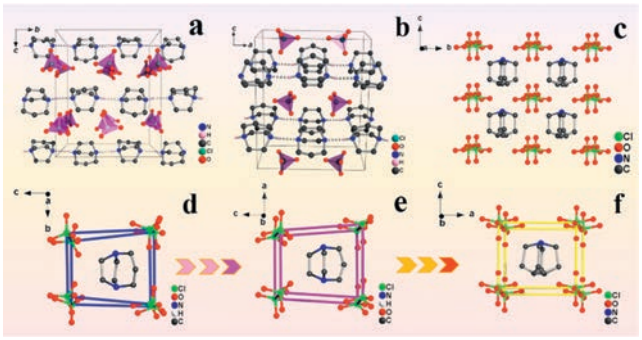

Fig. 2. The packing views of **1** in ferroelectric phases (a, d) 173 K, (b, e) 293 K and (c, f) paraelectric phase 393 K.

In phase I, the stacking diagram of **1** (Fig. 2a) shows that the monoprotonated [1,5–3.2.2-Hdabcn]$^+$ cations are connected through the hydrogen bonds N–H···N to form a wavy one-dimensional chain, this connection is also found in similar molecular ferroelectrics [1,4–2.2.2-dabco]ReO_4, [1,4–2.2.2-dabco]ClO_4 and [1,4–2.2.2-dabco]BF_4 [37,43,45], but unlike the ideal linear N–H···N hydrogen bonds in the perfectly spherical molecule 1,4–2.2.2-dabco. As shown in Fig. 2d, one organic amine cation is surrounded by eight anions, just like a twisted cage structure enclosing an organic cation.

To be noted, in phase II, the asymmetric unit consists of half deprotonated [1,5–3.2.2-H_2dabcn]$^{2+}$ cation, half unprotonated [1,5–3.2.2-dabcn] molecule, and one ClO_4^- anions. Different from the head-to-tail hydrogen-bonding interactions of monoprotonated [1,5–3.2.2-Hdabcn]$^+$ in phase I, the deprotonated [1,5–3.2.2-H_2dabcn]$^{2+}$ is connected with unprotonated [1,5–3.2.2-dabcn] molecule to for a dimer [1,5–3.2.2- H_2dabcn]$_2^{2+}$ by intramolecular hydrogen bond N–H···N. Then the dimers are further connected to form a wavy chain [1,5–3.2.2-H_2dabcn]$_n^{n+}$ through hydrogen bonds, Fig. 2b. The cage structure surrounding the cations becomes a relatively regular wedge-shaped hexahedron (Fig. 2e).

In phase III, **1** still crystallizes in the orthorhombic crystal system but adopts mmm point group with $Cmma$ space group ($a = 11.466(3)$ Å, $b = 13.468(4)$ Å and $c = 6.7503(19)$ Å, $\alpha = \beta = \gamma = 90°$). As shown in Fig. 2c, the cation and anionic are severely disordered, which makes the molecular configuration change from the original low-symmetry cage structure to a high-symmetry cage structure. At this stage, the hexahedron wrapping the cations also becomes more regular, presenting as a regular rectangle (Fig. 2f).

Compound **2** crystallizes in the polar space group $Pca2_1$ of $mm2$ at 293 K ($a = 17.9283(7)$ Å, $b = 6.9767(2)$ Å, $c = 8.5325(3)$ Å, $\alpha = \beta = \gamma = 90°$, Table S2 in Supporting information). As shown in Fig. 3a, the structure of **2** is constructed with the monoprotonated [1,5–3.2.2-Hdabcn]$^+$ cations and ReO_4^- anions, which are connected by the N–H···O hydrogen bond to form a discrete molecule. In the ReO_4^-, the Re–O bond lengths range from 1.701(4) Å to 1.717(4) Å, and the O–Re–O bond angles range from 108.2(3)° to 110.7(2)°, indicating that the anion group is an irregular tetrahedral structure. Compound **2** has a zero-dimensional structure in phase I, which is different from the other spherical molecules, such as [1,4–2.2.2-dabco]ReO_4 and [1,4–2.2.2-dabco]ClO_4, in which the cations are 1D chains connected by hydrogen bonds [37,43].

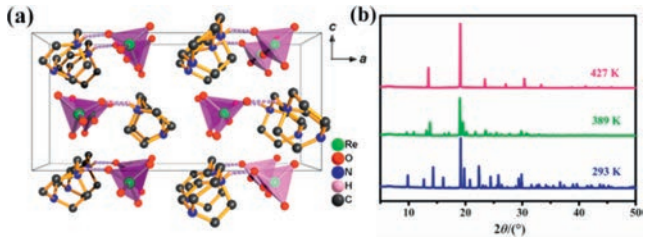

Fig. 3. (a) Crystal structure of **2** in the ferroelectric phase at 293 K. (b) PXRD tests of the powder sample of **2** at different temperatures.

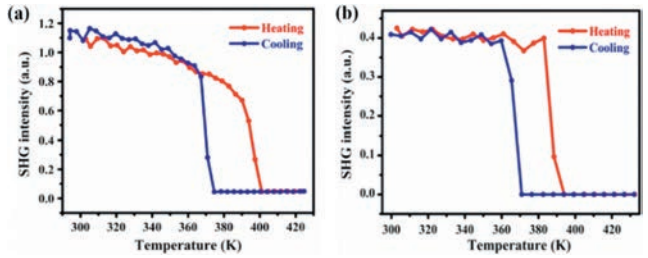

Fig. 4. Temperature dependence of SHG signals for polycrystalline samples (a) **1** and (b) **2**.

In high-temperature phase II, due to the highly disordered molecules making crystal structure solution difficult, the variable temperature PXRD tests at 390 K and 427 K were performed for **2**. As shown in Fig. S2b, the XRD pattern at 293 K is in good agreement with the single crystal simulation data from the room temperature. Compared with 293 K, the diffraction peaks at 390 K are significantly reduced, indicating that compound **2** has undergone a structural phase transformation and entered a new phase (Fig. 3b). Based on the PXRD data at 390 K, it was deduced that compound **2** crystallizes in the orthorhombic crystal system (Fig. S3a in Supporting information), and the space group with the maximum probability speculated by the Pawley refinements is *Pmm*2. This is also consistent with the subsequent SHG activity response.

Compared with the two groups of peaks at phase I and II, the diffraction peaks at 427 K (phase III) are significantly reduced, and the diffraction characteristics are very similar to those of the paraelectric phases found in the *quasi*-spherical structures [quinuclidinium][X] (X = ReO_4, ClO_4, and PF_6), and [2.2.2-dabco]ReO_4 [37,46]. The PXRD data at 427 K also revealed that **2** may be crystallized in the tetragonal system (Fig. S3b in Supporting information), and the space group with the maximum probability speculated by the Pawley refinements is *P*4/*mmm*.

The polar space groups are usually accompanied by SHG activity, and the centrosymmetric space group shows SHG inactivity. In general, the ferroelectric-paraelectric phase transition is usually accompanied by a transition of crystal structure from the polar space group to the centrosymmetric space group, therefore, the temperature-dependent SHG response measurement of compounds **1** and **2** was performed. As shown in Fig. 4a, compound **1** shows an obvious SHG activity below 390 K, suggesting a polar phase, and consistent with the ferroelectric space groups $Pna2_1$, $Pmn2_1$ in phases I, II. With the increase in temperature, the SHG signal intensity rapidly drops to zero at around 400 K and remains stable thereafter, which demonstrates a centrosymmetric crystal structure, corresponding to the centrosymmetric space group *Cmma* in phase III.

As shown in Fig. 4b, it can be seen that the SHG signal of compound **2** is active before T_2, this is consistent with its crystallization in the non-centrosymmetric space groups $Pca2_1$ (phase I) and *Pmm*2 (phase II). When the temperature reaches the vicinity of T_2, the SHG intensity value suddenly dropped to zero, which implies that compound **2** enters a centrosymmetric space group. Combined with the variable temperature PXRD, it should be the centrosymmetric space group of *P*4/*mmm*. Therefore, combined with SHG and crystal structure analysis, compounds **1** and **2** undergo the *mmmFmm*2 and *P*4/*mmmFmm*2 type ferroelectric phase transitions, respectively [47].

Piezoresponse force microscopy has extremely high spatial resolution and can realize the visualization of ferroelectric domain structures at the microscopic nanoscale, which is a powerful tool to demonstrate the existence of nanoscale ferroelectricity. Figs. 5a and b show the PFM phase, topography, and amplitude images for the thin films of **1**. The distinct tonal domain structures in the phase image suggest the existence of antiparallel domains. A clear domain wall can be observed in the amplitude map, transforming the original single-domain structure into a double-domain structure, where the intensity of the piezoelectric signals is very close, proving the existence of 180° antiparallel domain structure. Figs. 5c

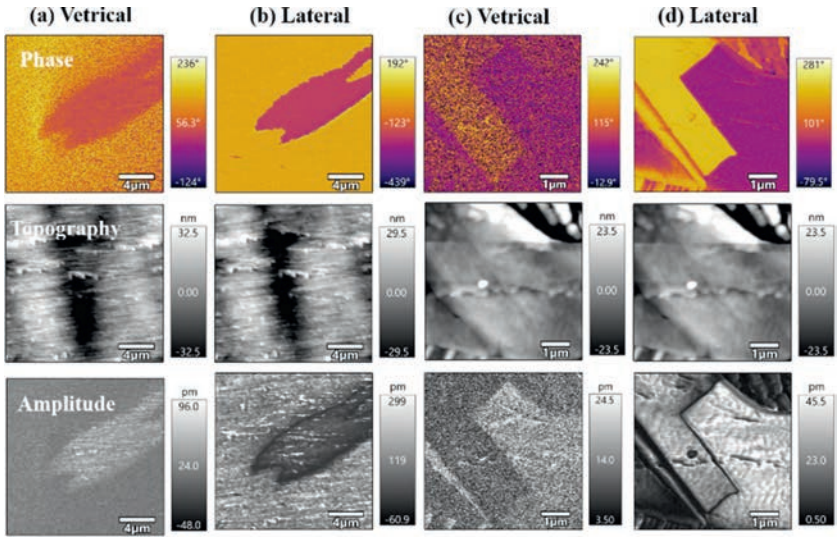

Fig. 5. The PFM phase, topography, and amplitude images for the thin film of (a, b) **1** and (c, d) **2** at one region with 180° domain in the (a, c) vertical and (b, d) lateral components, respectively.

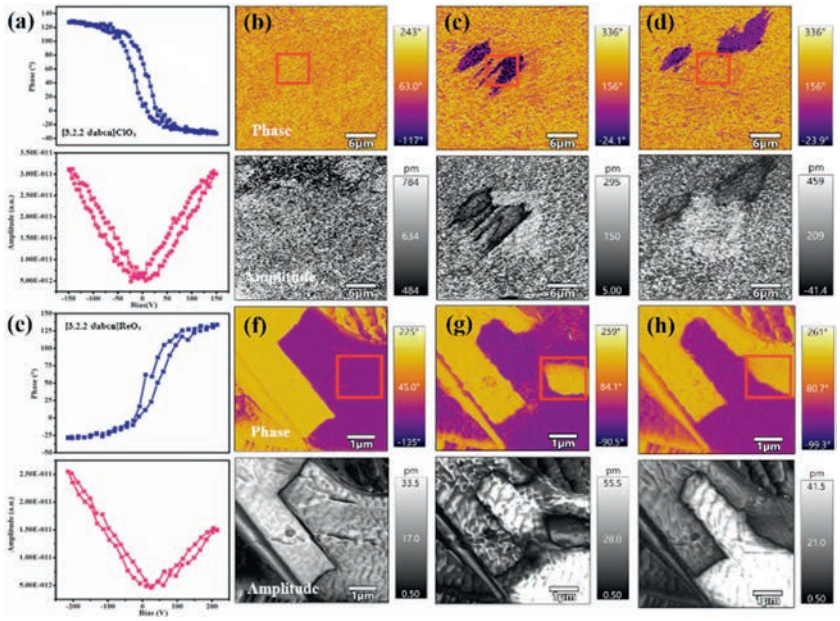

Fig. 6. Phase and amplitude signals as functions of the tip voltage for a selected point, showing a hysteresis loop and a butterfly curve of (a) **1** and (e) **2**. Vertical PFM phase (top) and amplitude (down) images of the films for **1** and **2**: (b, f) Initial state; (c, g) After the first polarization reversal by applying +110 V and +120 V tip bias. (d, h) After the succeeding back-switching produced by applying −110 V and −120 V tip bias.

and d show the vertical and lateral components of 180° domain structure for the thin films of **2**, the phase diagram clearly shows two antiparallel domains, and the piezoresponse of adjacent domains are similar in the amplitude images. This provides sufficient evidence for the existence of 180° antiparallel domains.

The spontaneous polarization of electrical switching is the most essential feature of ferroelectrics. It reveals the repeated switching of ferroelectrics between two or more polarization states under the excitation of the external electric field. Therefore, the local PFM-based hysteresis loop measurement was performed to verify the ferroelectric characteristic of **1** and **2**. In Figs. 6a and e, the typical hysteresis loops and butterfly curves of phase and amplitude as a function of the bias tip voltage indicate the successful polarization switching of domains. The local coercive voltages of **1** and **2** were estimated to be about 13 V and 25 V by averaging the minima of the amplitude loops.

For a more intuitive observation of the switching process of domains, the localized polarization operations were performed on thin films of **1** and **2** in the as-grown state. First, a single domain region was selected as the initial state for polarization switching tests, as shown in the red boxes of Figs. 6b and f, and then, a DC tip bias of +110 V and +120 V were applied to the selected areas on the thin films. It can be clearly observed that a new domain appears in the phase diagram, and an obvious domain wall also appears in the amplitude diagram, confirming that the ferroelectric domain has completed a polarization reversal (Figs. 6c-g). Finally, when an opposite bias of −110 and −120 V was applied, the polarization direction of the selected region (Figs. 6d and h) can be reversed back, indicating that the polarization of these domains can be switched reversibly and repeatedly.

In summary, we have successfully designed and prepared two molecular ferroelectrics [1,5–3.2.2-Hdabcn]ClO_4 (**1**) and [1,5–3.2.2-Hdabcn]ReO_4 (**2**), which show two high-temperature phase transitions. The variable-temperature single crystal structures revealed compound **1** undergoes a *mmmFmm*2 type ferroelectric phase transition near 380 K. While compound **2** crystallizes in the polar point group *mm*2 in both phase I and phase II, and the centrosymmetric point group 4/*mmm* in phase III, with a 4/*mmmFmm*2 type ferroelectric phase transition near 396 K. At room temperature, the switching of ferroelectric domains and rectangular P-E hysteresis loops were successfully achieved on the polycrystalline films of **1** and **2**. In addition, the low coercive voltages of 13 V (**1**) and 25 V (**2**) and easy domain reversal make them considerable potential for practical applications.

Declaration of competing interest

The authors declare that they have no known competing financial interests or personal relationships that could have appeared to influence the work reported in this paper.

Acknowledgments

This work was supported by the National Natural Science Foundation of China (Nos. 21865015, 22071094 and 22075123) and the Department of Science and Technology in Jiangxi Province (No. 20213BCJ22055).

Supplementary materials

Supplementary material associated with this article can be found, in the online version, at doi:10.1016/j.cclet.2023.108809.

References

[1] M.E. Lines, A.M. Glass, Principles and Applications of Ferroelectrics and Related Materials, Oxford University Press, 2001.
[2] D.W. Fu, H.L. Cai, Y. Liu, et al., Science 339 (2013) 425–428.
[3] S. Horiuchi, Y. Tokunaga, G. Giovannetti, et al., Nature 463 (2010) 789–792.
[4] W.Q. Liao, D. Zhao, Y.Y. Tang, et al., Science 363 (2019) 1206–1210.
[5] C. Shi, J.J. Ma, J.Y. Jiang, et al., J. Am. Chem. Soc. 142 (2020) 9634–9641.
[6] Y.Y. Tang, Y. Xie, Y.L. Zeng, et al., Adv. Mater. 32 (2020) 2003530.
[7] W. Li, Z. Wang, F. Deschler, et al., Nat. Rev. Mater. 2 (2017) 1–18.
[8] A.R.J.P. Ubbelohde, I. Woodward, Proc. Roy. Soc. 185 (1946) 448–465.
[9] D. Damjanovic, Reports Progress Phys. 61 (1998) 1267.
[10] A.J. Lovinger, Ferroelectric Polym. Sci. 220 (1983) 1115–1121.
[11] R.B. Meyer, Mol. Cryst. Liquid Crystal. 40 (1977) 33–48.
[12] A.S. Tayi, A. Kaeser, M. Matsumoto, et al., Nat. Chem. 7 (2015) 281–294.
[13] S. Horiuchi, F. Ishii, R. Kumai, Y. Okimoto, et al., Nat. Mater. 4 (2005) 163–166.
[14] M.H. Lee, D.J. Kim, J.S. Park, et al., Adv. Mater. 27 (2015) 6976–6982.
[15] C. Zhou, H. Yang, Q. Zhou, et al., Ceram. Int. 39 (2013) 4307–4311.
[16] J. Rödel, W. Jo, K.T. Seifert, et al., J. Am. Chem. Soc. 92 (2009) 1153–1177.

[17] J. Chen, J. Cheng, J. Guo, et al., J. Am. Chem. Soc. 103 (2020) 374–381.
[18] X. Wang, J. Wu, D. Xiao, et al., J. Am. Chem. Soc. 136 (2014) 2905–2910.
[19] J. Park, M. Lee, D. Kim, et al., J. Korean. Phys. Soc. 66 (2015) 1106–1109.
[20] K.J. Choi, M. Biegalski, Y. Li, et al., Science 306 (2004) 1005–1009.
[21] E. Sawaguchi, J. Phys. Soc. Jpn. 8 (1953) 615–629.
[22] C. Shi, X. Zhang, Y. Cai, et al., Angew. Chem. Int. Ed. 127 (2015) 6304–6308.
[23] Z.Y. Du, T.T. Xu, B. Huang, et al., Angew. Chem. Int. Ed. 127 (2015) 928–932.
[24] S. Chen, R. Shang, B.W. Wang, et al., Angew. Chem. Int. Ed. 54 (2015) 11093–11096.
[25] R. Gao, S.E. Reyes-Lillo, R. Xu, et al., Chem. Mate. 29 (2017) 6544–6551.
[26] S. Anwar, D. Pinkal, W. Zajaczkowski, et al., Sci. Adv. 5 (2019) eaav3489.
[27] A. Chouprik, R. Kirtaev, M. Spiridonov, et al., ACS Appl. Mater. Interfaces 12 (2020) 56195–56202.
[28] S. Tu, F. Ming, J. Zhang, et al., Adv. Mater. 31 (2019) 1806860.
[29] Q. Zheng, C. Bao, W. Guo, et al., Nat. Commun. 7 (2016) 11215.
[30] C. Qiu, B. Wang, N. Zhang, et al., Nature 577 (2020) 350–354.
[31] A. Fernandez, M. Acharya, H.G. Lee, et al., Adv. Mater. 34 (2022) 2108841.
[32] D. Pierangeli, M. Ferraro, F. Di Mei, et al., Nat. Commun. 7 (2016) 10674.
[33] C.F. Wang, N. Wang, L. Liu, et al., Chin. Chem. Lett. (2022) 108051.
[34] Y. Fan, S. Deng, T. Li, et al., Chin. Chem. Lett. (2022) 107796.
[35] Q. Pan, Z.B. Liu, Y.Y. Tang, et al., J. Am. Chem. Soc. 139 (2017) 3954–3957.
[36] Y.M. You, W.Q. Liao, D. Zhao, et al., Science 357 (2017) 306–309.
[37] Y.Y. Tang, P.F. Li, W.Y. Zhang, et al., J. Am. Chem. Soc. 139 (2017) 13903–13908.
[38] H.Y. Zhang, Y.Y. Tang, P.P. Shi, et al., Acc. Chem. Res. 52 (2019) 1928–1938.
[39] C.K. Yang, W.N. Chen, Y.T. Ding, et al., J. Am. Chem. Soc. 141 (2019) 1781–1787.
[40] C. Xu, W.Y. Zhang, Q. Ye, et al., Inorg. Chem. 56 (2017) 14477–14485.
[41] J. Harada, N. Yoneyama, S. Yokokura, et al., J. Am. Chem. Soc. 140 (2018) 346–354.
[42] L. Zhou, P.P. Shi, X.M. Liu, et al., NPG Asia. Mater. 11 (2019) 15.
[43] Y.Y. Tang, W.Y. Zhang, P.F. Li, et al., J. Am. Chem. Soc. 138 (2016) 15784–15789.
[44] Z.H. Wei, Z.T. Jiang, X.X. Zhang, et al., J. Am. Chem. Soc. 142 (2020) 1995–2000.
[45] P.P. Shi, Y.Y. Tang, P.F. Li, et al., J. Am. Chem. Soc. 139 (2017) 1319–1324.
[46] J. Harada, T. Shimojo, H. Oyamaguchi, et al., Nat. Chem. 8 (2016) 946–952.
[47] K. Aizu, J. Phys. Soc. Jpn. 27 (1969) 387–396.